IPP-Report

IPP Max-Planck-Institut für Plasmaphysik

A. Lorenz, W. Beck, P. Cierpka, L. Hu,
P.T. Lang, R.S. Lang, G. Weber

Optimised Pellet Guiding to the Magnetic High Field Side of ASDEX Upgrade

IPP 1/317
Oktober 1998

OPTIMISED PELLET GUIDING TO THE MAGNETIC HIGH FIELD SIDE OF ASDEX UPGRADE

A. Lorenz, W. Beck, P. Cierpka, L. Hu*, P.T. Lang, R.S. Lang, G. Weber

Max-Planck-Institut für Plasmaphysik
EURATOM Association
Boltzmannstr. 2, 85748 Garching, Germany

ABSTRACT

Efficient refueling is one of the basic requirements to sustain thermonuclear plasmas in future tokamak based fusion grade reactors. Although injection of cryogenic deuterium pellets from the magnetic high field side (HFS) was predicted to have more potential /1/ and at ASDEX Upgrade found to be more efficient /2/ than injection from the low field side (LFS), the technical implementation of HFS refueling remains critically restricted to low velocities (v = 240 m/s) due to limited accessibility of the high field side of the torus. The maximum speed available by the ASDEX Upgrade centrifuge /3/ is v = 1200 m/s. The required optimisation of the system guiding the pellets to the HFS is suggested by analysing the components (funnel and curved guiding tube), studying their characteristics and the physical processes involved. Firstly, impact tests on flat targets to emulate impact in a funnel were performed. Pellets were not reflected but found to quasi-slide along the inner surface of the target after the first impact. The impact velocity perpendicular to the target was found to control the survival of the pellets. At a velocity of about 42 m/s all pellets survived one or more impacts under angles of 3° - 6°. An impact angle of 2° was extrapolated to ensure pellet survival at v = 1200 m/s. Accordingly, a new funnel was designed.

A hidden impact parameter consisting in a transient loss of wall contact and impact onto the opposite tube wall at turning points of the tube curvature was disclosed. This appeared to be more important than continuous centripetal forces acting on a pellet going through a smooth bend. Consequently, a new configuration is proposed which is based on a permanent curvature of both, funnel and guiding tube to avoid the loss of wall contact In this case a minimum curvature radius of R > 0.6 m would suffice to reach v = 1200 m/s. The new system is designed to have a full vacuum mantling to ensure only one pellet impact throughout the system in the funnel. The cross-sectional shape of the tube, the internal tube size and tube length are discussed and their optimum characteristics are found. Of particular importance for plasma density control is a short guiding tube length found to control the overall duration of the pellet transfer from extrusion to the plasma for high pellet velocities.

* present address: Dptm. Fusion Facility, Naka Fus. Res. Estab., JAERI, Naka-gun, Ibaraki-Ken, 3110193, Japan

TABLE OF CONTENTS

1. INTRODUCTION

Injection of frozen pellets made from hydrogen isotopes is regarded as an advanced fueling technique for fusion devices and planned fusion reactors. Standard injection systems where pellets are injected from the outside into the plasma (LFS) were found to suffer from strong efficiency degradation in the presence of auxiliary heating /2/. However, injecting the pellets from the inboard side, i.e. the magnetic high field side (HFS) of a tokamak this disadvantage can be overcome. At the same velocity, HFS-pellets can penetrate into the plasma much deeper than LFS-pellets due to a "high beta"-plasmoid compassing the ablation cloud of an injected pellet /1/. The plasmoid forms when electron thermal energy of the hot background plasma is transferred along field lines to the cold pellet gas shield much faster than the shield expands (with ion sound speed) /3/. In tokamaks the diamagnetic plasmoid drifts in major radius direction dominated by ∇B. Consequently, a large part of the pellet mass, when injected from the LFS, is forced back out to the edge without reaching the high density, high temperature core. In contrast, during injection from the HFS the plasmoid splitters drift in the same direction, but in this case toward the plasma centre, a fact which is rather favourable for refueling fusion grade plasmas such as ITER by pellet injection.

On the other hand, the accessibility of the magnetic high field side of tokamaks, here ASDEX Upgrade, is very limited requiring a pellet guiding system and restricting the maximum pellet velocities. In recent experiments at ASDEX Upgrade pellets were successfully injected with $v = 240$ m/s, while the maximum speed made available by the injector, i.e. the centrifuge was $v = 1200$ m/s /4/. Achieving injection at $v > 1000$ m/s would enable to study the speed dependence for penetration of HFS-pellets, not performed experimentally yet. This too may be consequential for the capability of refueling fusion grade plasmas.

The currently installed pellet guiding system on ASDEX Upgrade consisting of a funnel and a guiding tube requires thorough analysis and improvements to gain access to pellet velocities $v > 1000$ m/s. It is this optimisation of the pellet guiding which we focus on in this report.

2. CURRENT OPERATION SCENARIO

After successful HFS-injection of D_2-pellets using a blower gun ($v = 130$ m/s) /5/ a preliminary pellet transport system was prepared for the centrifuge. This injector has several advantages with respect to the blower gun: the higher pellet speed, higher pellet injection rate of up to 70 Hz and injection of 3 pellet sizes (10^{20} to $4 \cdot 10^{20}$ D-atoms).

The centrifuge based preliminary pellet transfer system is displayed in Fig 1. At $v = 240$ m/s the centrifuge has a total angular scatter of $\pm 4°$ /4/, such that pellets leaving the centrifuge must be captured by a funnel. The scatter results in a 60 mm wide, fan shaped pellet beam at the

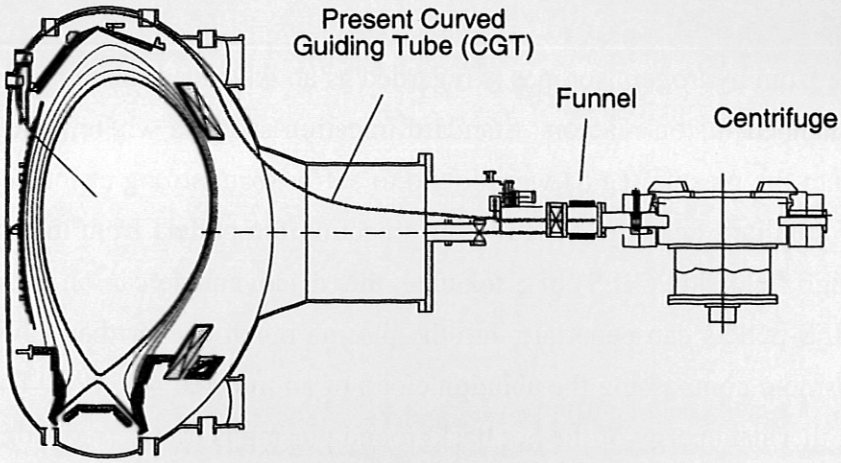

Fig. 1

Pellet transfer system to the magnetic high field side of ASDEX Upgrade. Pellet injection is performed under 44° to the horizontal plane.

funnel entrance. The beam width has to be reduced by a factor of ~10 to transfer the pellets into a Ø7 mm guiding tube. Therefore the funnel width converges from 60 to 6 mm over a length of 0.6 m to give a acceptance ±2°. The funnel forces pellet impact under up to 5° on one side and 7° on the other. The funnel has a rectangular cross-section with a height of 5 mm throughout. The funnel surface is made of Viton® thought to dampen the impact. Pellets leaving the funnel fly freely through an open torus shutter into the ~5 m long, flexible teflon tube leading to the upper inner side of the torus and ending between two carbon tiles under 44° to the horizontal plane. The first two meters of the tube can be moved vertically by a pressurised switch to change to LFS pellet injection. The restricted space available resulted in strong bends (R_{min} = 0.35 m) and frequent turning points in the tube geometry shown schematically in Fig. 2. The pellets have to withstand both, centripetal forces in bends and impacts on a tube wall at turning points. This is emphasised by the unknown trajectory along which the pellets propagate inside the guiding tube which may be even a spiral and lead to an irreproducible entry into the plasma /11/.

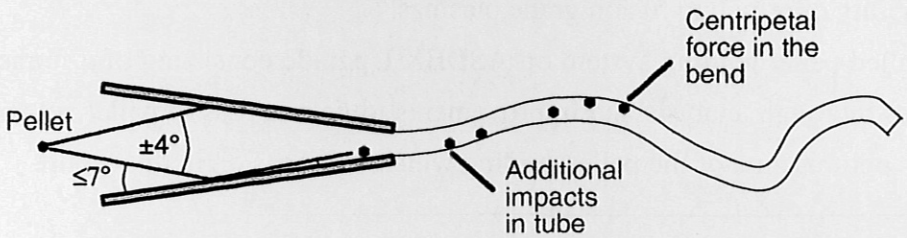

Fig. 2

Geometry of pellet scattering and funnel acceptance

During the previous experimental campaign large sized D_2-pellets (1.9×1.9×2.0 mm³) were reliably injected with a velocity of 240 m/s from the HFS of the torus losing only a few pellets /6/. A limitation of this configuration was found after HFS pellets with v = 560 m/s did not enter the plasma in contrast to LFS pellets which only had to pass the funnel but not the guiding tube. This conclusion was drawn from the fact that after HFS-injection no significant plasma density rise was observed but only a gas puff with very small fragments of D_2-ice whereas a small stepwise density rise was measured during LFS-injection. The frequency of the centrifuge was altered to determine the pellet destruction limit of the non-optimised HFS-injection set-up. The limit was found at v ≈ 400 m/s.

3.OPTIMISATION

The speed limitation for HFS-pellets has obviously three reasons: the pellet impact strength, the funnel to capture the pellets at the exit of the injector and a guiding tube to transfer the pellets to the HFS. Each component in turn depends on several parameters an overview of which is given in Table 1. Aim of the optimisation is a pellet guiding system permitting to reach 1200 m/s.

Element	**Parameter**	**Current Configuration**
Pellet Impact Strength	Temperature on ejection	6 - 7 K
	Composition	99.8% D_2
	Shape	Cube
	Size	1.9 x 1.9 x 2 mm^3
Funnel	Shape	plane
	Length	0.6 m
	Surface	Viton®
Guiding tube	Minimum curvature radius	0.35 m
	Internal diameter	7 mm
	Cross section geometry	round
	Length	~ 5 m

Table 1. Parameters controlling the survival of HFS-pellets during transfer from the centrifuge to the HFS of the torus. In the right column parameters of the currently installed configuration are given.

3.1. The pellet impact strength

3.1.1. Pellet temperature

The guiding of D_2-pellets is complicated by their inherent low yield strength /7/ displayed in Fig.3. This curve is valid for static uniaxial tension on a D_2-sample. According to /7/ the region between T = 4 -12 °K shows little change around an average strength of 5 bar. Fracture in this region occured only with preceding plastic deformation (1-7%) in form of microscopic cracks The continuity with T is significant because pellets in the centrifuge have T ~ 6 K just prior to

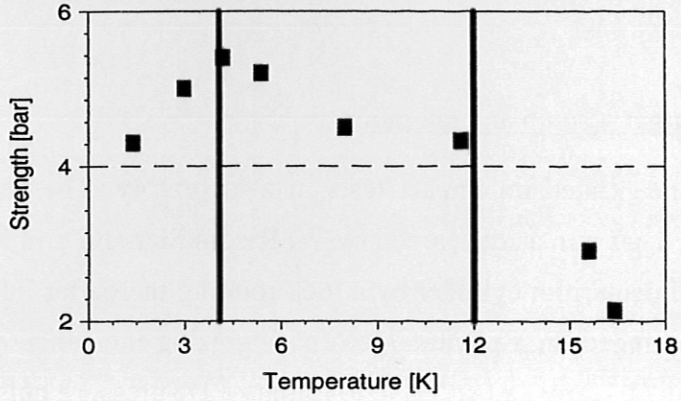

Fig. 3

Yield strength of cryogenic D_2 as a function of temperature. Measurements by Bolsch-yutkin et al. /7/.

ejection, whereas pellets extruded in the gas gun used for impact tests described below had T ~ 10 °K. For simplicity, a possible variation of pellet quality within the range T = 4 - 12 K will be ignored in this report.

Considering pulsed interaction of solid D_2 with targets such as the rotor blade of the centrifuge during acceleration pellets have been measured to withstand short-term (t < 1ms) stresses of 13 bar /4/. On an even shorter time scale of 1 μs as in grazing incidence impacts they should survive contact loads of 50 - 100 bar /8/.

3.1.2. Pellet composition

The pellet strength depends also on the amount of impurities. While the D_2-sample tested in Fig.3 contained 99.3% D_2 with unknown impurities, tensile strength experiments using H_2-pellets by Alexeeva et al. /8/ showed that the tensile strength could be increased by planting O_2 and N_2 into a H_2-pellet. The optimum was found for 0.1% N_2 with an increase by a factor of 1.5 - 2 up to 10 bar. The temperature of the samples was not specified. The strength of pellets produced at ASDEX Upgrade (99.8% D_2 containing ~ 0.2% HD and traces of N_2 and O_2 /9/) is discussed in sections 3.2. and 3.3., but only in terms of compressive loadings.

3.1.3. Pellet size and shape

The size of the pellet is important with regard to the contact area during impacts. As the contact pressure p = F/A is proportional to the pellet size, a_p (one side of a cube, or length of a cylinder), i.e. the contact area, the larger pellets are expected to break at lower speeds than smaller pellets. The cubic pellet shape for centrifuge pellets was chosen because of the pellet accelerating procedure. After cutting the pellet falls about 2 cm into a stop cylinder from where it is transferred on to the rotor blade and ejected /4/. A cubic pellet will land on one of its squares, whereas a cylinder might roll along its curvature making the pellet position on the acceleration arm irreproducible. In impact tests described below cylindrical pellets were shot using a gas gun. Thus the initial pellet position was fixed in the gun barrel.

3.2 The funnel

3.2.1. Impact tests on a plane target - setup and operation

Optimisation of the funnel concentrated on impact tests in a laboratory. The study was performed using an extrusion based gas gun as developed by W. Riedmüller /10/ and K. Büchl /11/. Pellets are cut from a solidified deuterium cylinder by a lock rotating thereafter into firing position. After firing the pellets impinged on a plane target under grazing incidence angles. Firing was executed by shortly opening (1 - 2 ms) a fast valve to initiate a D_2-pressure pulse of p = 20 -

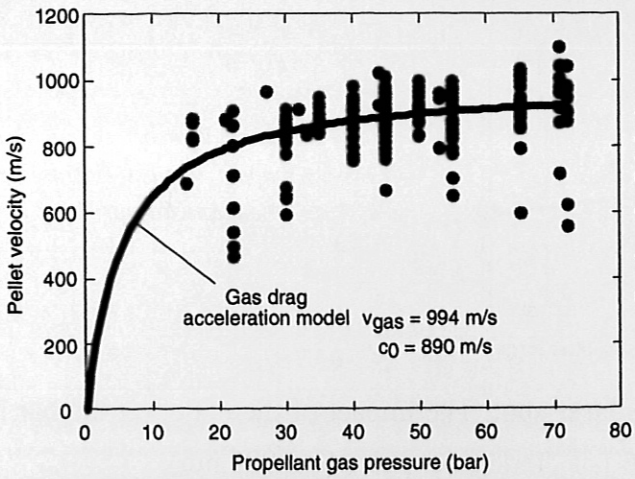

Fig. 4: Pellet velocity as a function of propellant gas pressure p using D_2 as propellant gas.

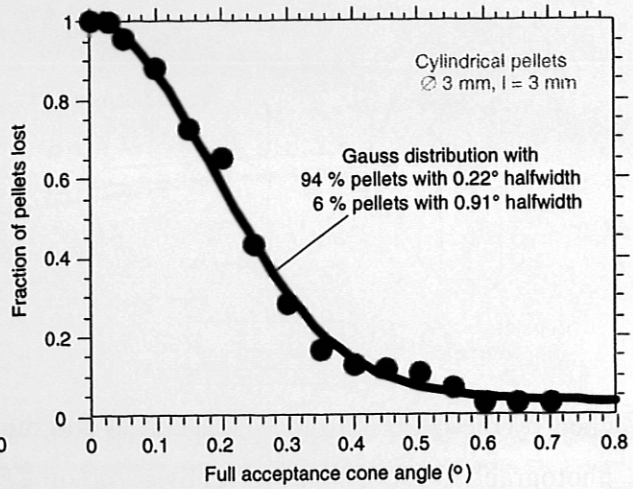

Fig. 5: Pellet scatter of the fast gun used in impact test. Barrel length 360 mm.

40 bar. Fig.4 shows the pellet velocity as a function of p using D_2 as propellant gas. The velocity band of the gun narrowed during the course of the study from of 500 - 1000 m/s to 700 - 900 m/s. This was mostly attributed to wear in the propellant valve mechanics and the gun lock improving the speed reproduciblity.

The propellant pressure is the main tool to control the pellet velocity. However, velocities below 500 m/s could only be achieved using p = 5 - 10 bar which was accompanied by insufficient heating of the lock cavity, i.e. inadequate removal of pellet ice freezing the lock due to the heat capacity of the propellant D_2-gas. The only other means of attaining velocities $v < 500$ m/s was to lower the breakaway pressure of the pellet by warming the lock before cutting the next pellet. A temperature rise from 10 to 12 K was necessary to reduce the speed by 50 m/s.

As can be seen from Fig.5 the FWHM of the scattering angle in the horizontal plane is ±0.22°. It must be noted that the distribution is not a single Gaussian but contains an additional component because about 6% of all pellets showed a scatter of ±0.91°. These pellets were not included in the analysis of the impact tests because they would hit the target at the front edge. In the vertical plane a spread of ±0.5° was detected. The pellets used were slightly larger (Ø3 mm, l = 3 mm) than those produced by the centrifuge which was useful for scaling the results to the centrifuge because a higher possibility of pellet damage was introduced.

The set-up of the measurements is shown in a schematic in Fig. 6. The pellets were passing light barriers before and after hitting the target to measure the respective velocities. The target was an aluminium bar which either had a smoothed aluminium or a glued-on Viton® surface. The bar could be rotated to provide an incidence angle $\alpha = 0$ to 10° with an accurracy of ±0.3°. After passing the target the pellet penetrated a paper target. A red diode laser on top of the bar is aligned parallel to it and pointing onto the paper target so as to provide a reference point relative to the pellet. The reflection angle, β, is found by measuring the distance between the hole pun-

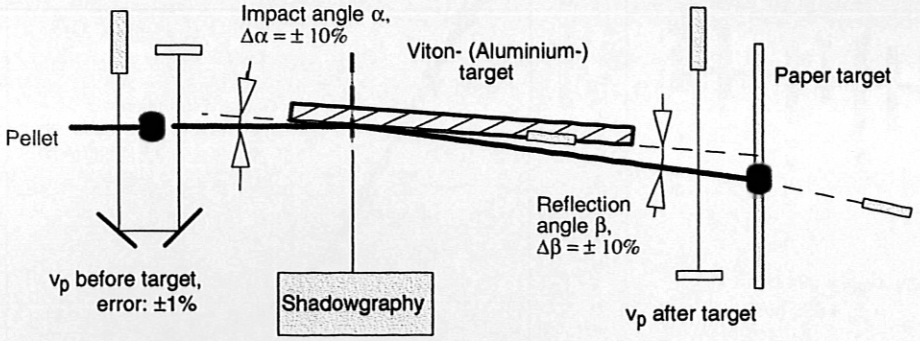

Fig. 6

Schematic of set-up for impact measurements on one plane target.

ched by the pellet into the paper target and the laser spot. The impact of the pellet on the bar is photographed using shadowgraphy based on a 50 ns diode laser pulse ($\lambda = 905$ nm).

The accuracy of the speed measurements was kept as low as ±1% due to a long base distance between the laser beams. The speed measurement after pellet impact was complicated by the spread in the impact position. However, recording the impact by means of the shadowgraph, the error of the post-target velocity did not exceed 4%.

3.2.2. Impact tests on a plane target - results and discussion

The main goal of the impact measurements was to find a working diagram of impact angle against pellet velocity, i.e to find a critical survival velocity at each angle. The state of the pellet after collision with the target was assessed in two categories, 1 - survived and 2 - destroyed, as seen in Table 2. By comparison to shadowgraphs, the paper diagnostics contained a significant error source. Pellets might be cut into two halves by an impact, and both halves would still be

PICTURES	PAPER TRACES
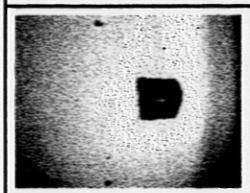 Category 1	One hole only of Ø3 mm and clear cut shape + possibly one hole of < Ø0.3 mm minor splitters.
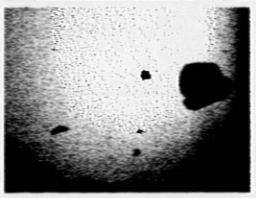 Error source	One hole >Ø2.5 mm with deformations and splitters of <Ø1. mm
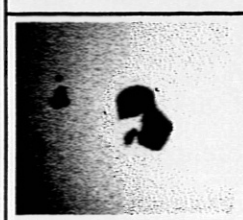 Category 2	All other possible traces from pellets intact before the target.

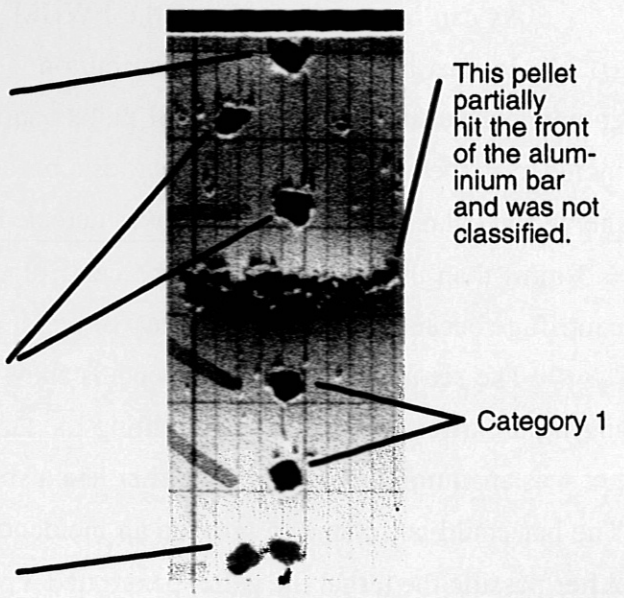

Table 2: Pellet state after collision with target: left - as observed by a shadowgraph, right - behind paper target. Shadowgraphs and paper traces belong to different pellets

flying as a whole through the paper. A destroyed pellet would mistakenly be identified as a surviving pellet. All doubtful paper traces were sorted into category 2, because shadowgraphy could not be used permanently due to the speed jitter of the gas gun, and resulting triggering jitter.

About 100 pellets were fired per angle ($\alpha \leq 6°$) and target, and their velocities were grouped into 5 - 10 average velocities, v_{av}. The selection of v_{av} was adapted to the density of shot velocities available in a specific range dv. The interval, $v_{av} \pm dv$, was aimed to be not larger than ±40 m/s. Then the fraction of survived pellets was calculated dividing the number of pellets in category 1 by the sum of pellets from categories 1 and 2 at each average velocity.

The difference between results aluminium and Viton® coated targets was negligible. Thus only results of the Viton® coated target are presented for clarity. Fig.7 shows the fraction of survived pellets as a function of average velocity for $\alpha = 3° - 6°$. Pellets hitting the target under $\alpha \leq 2°$ survived the impact up to v = 1080 m/s, the maximum attainable pellet speed. The average velocity was termed critical, v_c, at a survival probability of 0.8. This probability was chosen due to the statistical error introduced by forming velocity groups and consequently appearing data gaps due to irreproducible pellet velocities, in particular at v < 700 m/s.

The curves were fitted with one half of a Gaussian error function. Remarkably, almost identical fit parameters, i.e. gradients were detected for all angles but for a stronger peaking of the gradient with increasing impact angle. As can be seen the fits are idealised in that they ignore data tails, two in each curve, one at each end of the probability scale except for the lower tail at $\alpha = 3°$ and the upper at $\alpha = 6°$ due to the limited speed range of the gun. The tails are more ($\alpha = 4°$) or less ($\alpha = 5°$) expressed which is caused mainly by the varying density of available v_{av} across the range v = 400 - 100 m/s. The existence of the tails is thought to be due to the varying D_2-ice quality as the ice was stored in a cryostat before extrusion, each loading yielding 10 - 15 pellets with one pellet fired every 60 - 90 s.

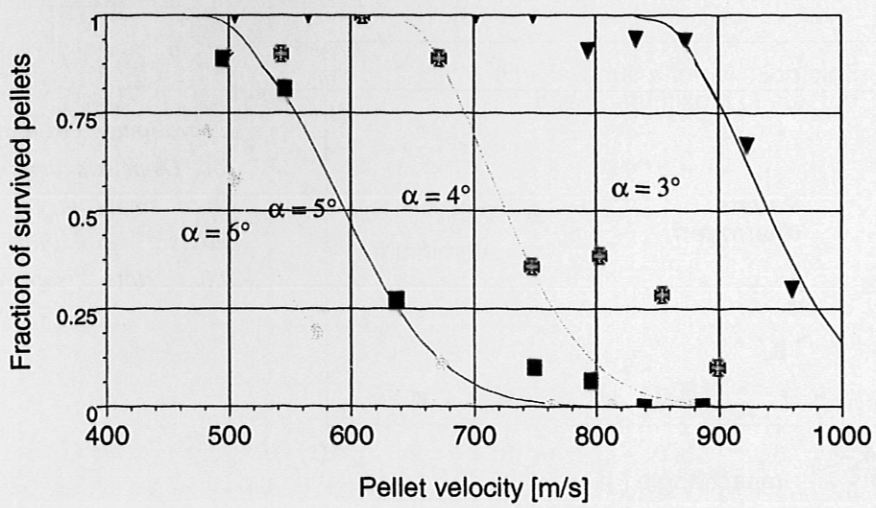

Fig. 7

Fraction of survived pellets as a function of incidence angle a and pellet velocity v.

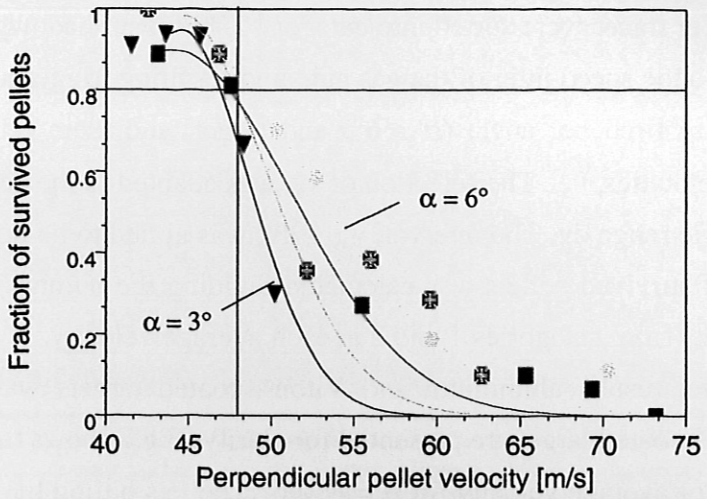

Fig. 8

Survival probability as a function of perpendicular pellet velocity. Legend is the same as in Fig. 7.

A remarkable effect of this study is evident in Fig.8 where a plot of survival probability as a function of perpendicular velocity for the same range $\alpha = 3° - 6°$ is displayed. The perpendicular component of the pellet velocity, $v_\perp = v \cdot \sin\alpha$, is the decisive parameter for the impact survival because a common velocity of $v_\perp \approx 48 \pm 0.9$ m/s at a probability of 0.8 is clearly seen for $\alpha = 3° - 6°$.

The critical speed of $v_\perp = 48$ m/s was very close to that of impact studies under normal incidence made by M. Thöner /12/ using pellets of T = 5 K. He obtained a speed interval of 48 - 62 m/s with the lower limit ascribed to 100% survival and the upper limit to 100% destruction. Strikingly, a pellet size of Ø1×0.9 mm in tests by Thöner /12/ means that the contact load during deceleration is a factor 3 larger in our tests. Similarly Combs et al. /13/ did not find any difference in critical velocity between Ø2.7 mm and Ø10 mm pellets in impact tests under $\alpha = 15° - 90°$. However, they obtained a much smaller critical speed ranging between $v_\perp = 20 - 35$ m/s. A possible reason for this might be the amount or the lack of impurities in the frozen D_2 used.

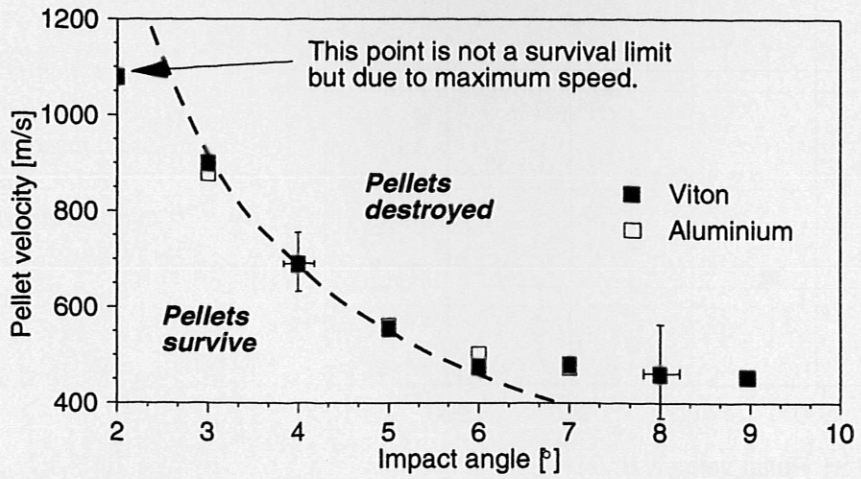

Fig. 9

Operational v-α-diagram for D_2-pellets impinging on a single target at a survival probability of 0.8. Note suppressed Zero.

The result of impact tests on a single target is summarised in a operational diagram in Fig.9 where the critical velocity is plotted as a function of impact angle. Also shown are critical speeds from pellets fired at angles of $\alpha \geq 7°$. They do not fit $v_\perp = 48$ m/s but display an increased impact strength most likely due to the small number of pellets fired at speeds below 450 m/s, therefore larger errors in v_{av} and the survival probability.

3.2.3. Impact tests with two successive targets

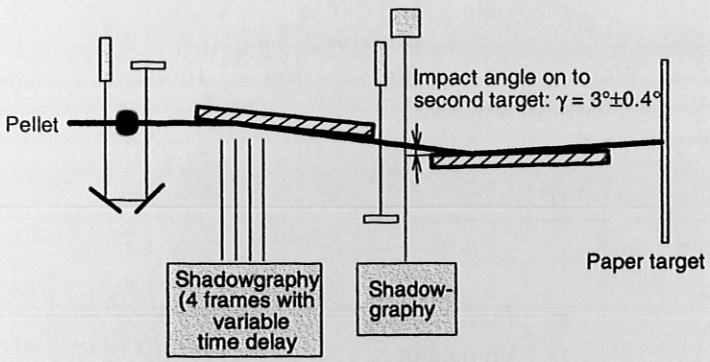

Fig. 10

Schematic of the set-up for 2-target impact tests.

Impact tests on two successive targets were carried out to find the uncertainty of single target tests, firstly, due to using the paper target as the categorising diagnostic, secondly, due to the brittleness of solid hydrogen capable of concealing damage at a microscopic level after the first impact. The set up is shown in Fig. 10 with the second target rigidly linked to the first. Both targets were aluminium bars without coating. The second impact angle was chosen at $\gamma \approx 3°$ to be comparable to α. A spread in the impact angle of $\Delta\gamma = \pm 0.4°$ could not be avoided due to a spread in β which will be discussed in the next section.

During the impact test α was varied between 3° - 5°. Results are shown in Fig. 11 where artificial fits for each α–γ-pair produced by multiplying the respective Gaussian fits from the single target tests are also plotted. Clearly the fits do not predict the survival probability after two targets most likely due to the aforementioned test motivation: the second impact highlights the inherent brittleness of the pellets and variations in the ice quality much stronger than a single collision. Expectedly the influence of the second target decreases as a increases. This is confirmed by the increase of $v_\perp$ from 42.5 m/s at $\alpha = 3°$ to 45 m/s at $\alpha = 5°$. More significant is the absolute reduction of v_c by 60 - 80 m/s suggesting that the survival probability of 0.8 used after a single impact is not adequate to determine a perpendicular destruction speed limit. Finding instead in Fig.7 v_c at a probability of 1 (using the Gaussian fits and ignoring the upper tails) a speed limit of $v_\perp = 42$ - 43 m/s is found for $\alpha = 3°$ - 6°.

Linking this result with the potential centrifuge speed maximum of v = 1200 m/s, a limiting impact angle of $\alpha \approx 2°$ is extrapolated. This is summarised in the bold curve in Fig. 12. Also shown is the result of preliminary double target impact tests with $\alpha = \gamma = 2°$, the point for sur-

Fig. 11

Fraction of survived pellets as function of impact angle α and pellet velocity for impact on two subsequent targets. Angle on to second target γ = 3°±0.4°.

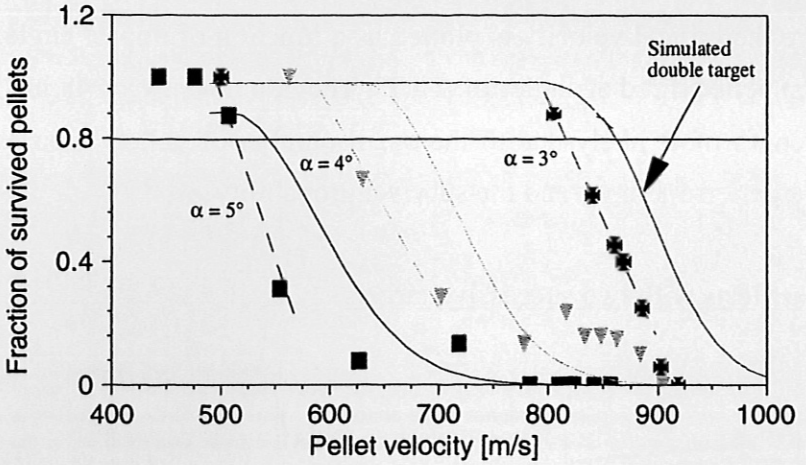

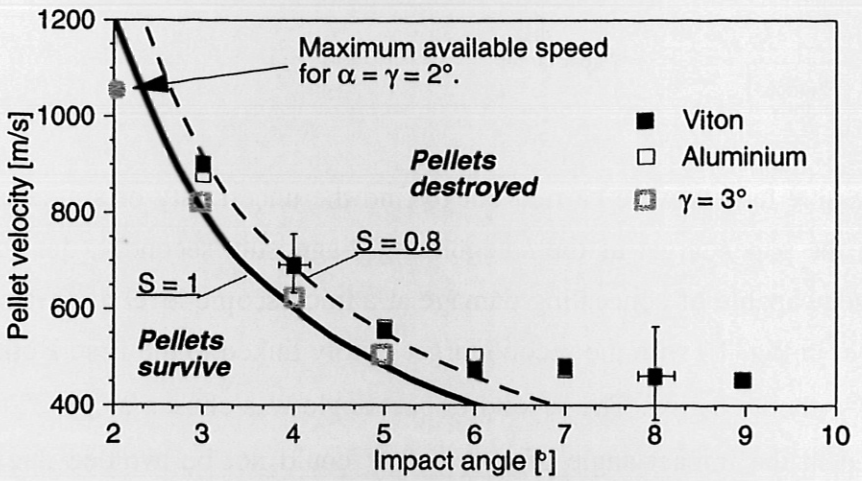

Fig. 12

Operational diagram of critical pellet velocity versus impact angle. Legend: S = 1 - survival fraction in single target tests, Note suppressed Zero.

vived pellets at the highest achievable speed of v= 1050 m/s. Altered gas gun operation should soon allow tests with v = 1200 m/s to confirm the extrapolation. As of now an impact angle of 2° will be regarded as the limit in both, funnel and guiding tube.

3.2.4. Pellet-target interaction

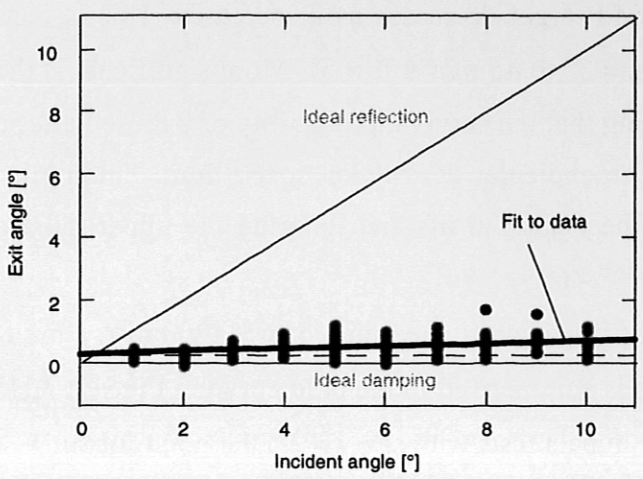

Fig. 13

Reflection angle β as a function of impact angle α. β is found by taking into account the pellet size corresponding to an offset of 0.2°.

A very important finding of the impact tests is displayed in Fig.13. The pellets are quasi-sliding after the impact on the target. Adjusting the data fit of the exit angle, β, through zero, an average "reflection" of $\beta = 0.4°$ is obtained. The differences in β between the target materials aluminium and Viton® and between intact and damaged pellets were of the order of $\Delta\beta = \pm 0.3°$. The deviation from ideal damping is very small, although perpendicular "reflection" velocities of ~5 m/s (at v = 500 m/s, α =5° - 6°) to ~9 m/s (at v = 1000 m/s, α = 2° - 3°) are encountered. It must be noted, that the graph integrates over intact and destroyed pellets as well as over pellet velocities.

A series of photographs taken from one pellet impact and shown in Fig. 14 reveals that strong evaporation (less at smaller impact angle) is taking place during contact of pellet and target. Part of the pellet is shaved off regardless of the orientation of the pellet with respect to the target before the impact. The pellet is not turning or rotating in its frame of reference due to the impact which suggests that the measured quasi-sliding is due to formation of a deuterium gas layer carrying the pellet. On the other hand, measurements of the post-target-velocity did not indicate pellet acceleration perpendicular to the target by the jet stream effect due to the gas layer.

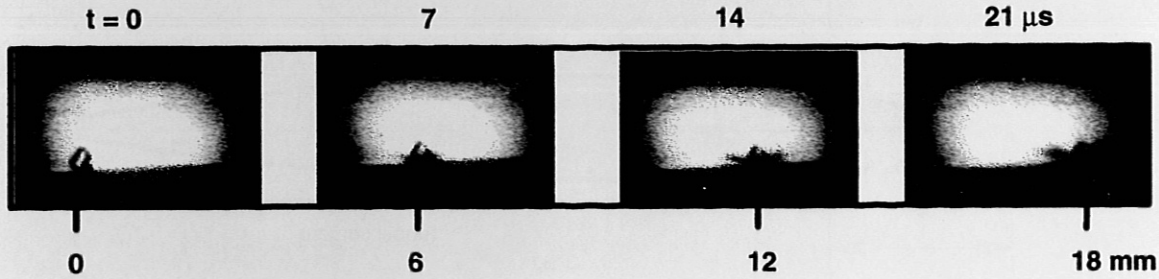

Fig. 14 Four frame photograph of the pellet impact at v = 817 m/s on a plane target under α = 4°. Often splitters break away instead of the shaving - depending on impact angle and temperature of the pellet.

The pellet-target interaction and the single impact destruction limit of $v_\perp = 48$ m/s have not been studied in detail yet. Below a first approach to the mechanics of the pellet impact is attempted for a centrifuge pellet ($a_p = 2$ mm). The longitudinal compression of the pellet, Δl, can be determined assuming an elastic process during decelaration from $v_\perp \sim 50$ m/s to zero. Using the definition of Young's module, ε, and the conservation of energy during the impact, Δl can be estimated as follows:

$$\Delta l = \sqrt{\frac{2 \cdot E_{kin} \cdot a_p}{\varepsilon \cdot A}} \qquad (1)$$

where $E_{kin} = 2$ mJ is the kinetic energy and A is the contact area of the pellet. The pellet compression by acceleration is ~ 70 µm at an acceleration of $a = -3.7 \times 10^7$ m/s². Using Hooke's law the maximum contact load on the pellet becomes 150 bar. The duration, T, of this process can be estimated using the first quarter period of an elastic oscillation:

$$\frac{d^2x}{dt} = -\frac{kx}{m} \quad \Rightarrow \quad T = \frac{2\pi}{\sqrt{k/m}}; \qquad (2)$$

where x = Δl, k the spring constant and m is the pellet mass. Finding k from Hooke's Law as 8.8×10^5 N/m, the quarter period is T/4 ≈ 2 μs. Then an average sound speed of $c_s \leq 1100$ m/s /14/ is not sufficient to transfer the impact compression through the whole pellet within 2 μs. However, this estimate depends strongly on how fast an evaporation cloud is formed and where the kinetic energy is absorbed.

To summarise, plastic deformation of the pellets was not observed, the energy seemed to be lost via evaporation and sputtering or shaving off of pellet portions. Very likely only a small part of the pellet is involved in the impact, and consequently responsible for its destruction.

3.2.5. Design of an optimised pellet funnel

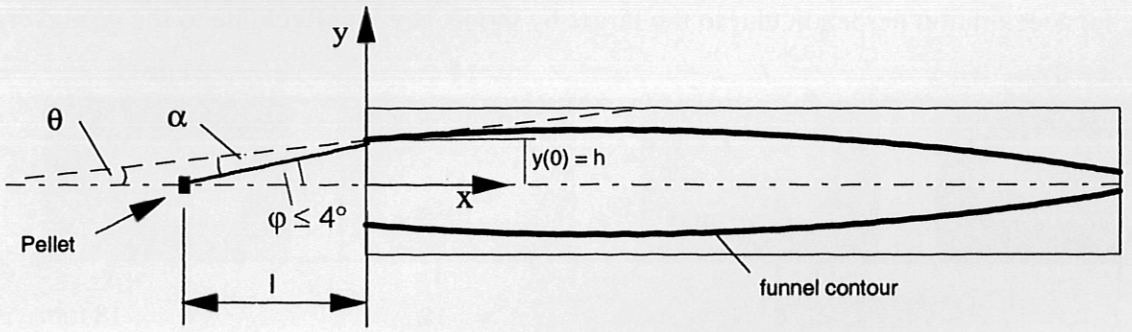

Fig. 15 Geometry for derivation of optimised funnel contour to reach φ ≤ 2°.

In order to satisfy the condition derived in the impact study, α ≤ 2°, the shape of the funnel can not be straight when accepting a pellet fan of ±4°. An optimised contour can be derived as shown in Fig. 15 where α = 2° is the constant angle of impact onto the funnel contour sought after, φ is half of the pellet scattering angle by the centrifuge, θ is the angle of the tangent to the element of the curve sought for, y(0) = h is the half width of the funnel at the entrance. Assuming that for small θ the arc of θ ~ tgθ and respectively φ ~ tgφ, two equations are valid:

$$\frac{dy}{dx} = \frac{2\pi\cdot(\varphi-\alpha)}{360} \qquad (3a), \qquad \varphi = \frac{y\cdot 360}{2\pi\cdot(x+l)} \qquad (3b),$$

which combine to:

$$\frac{dy}{dx} - \frac{y}{x+l} + 0.01745\cdot\alpha = 0 \qquad (4).$$

The solution of this can be found analytically:

$$y = -0.01745\times\theta\times(x+l)\times ln[(x+l)/l]+(x+l)\times h/l \qquad (5)$$

Based on a 6 mm width required at the funnel exit to fit the guiding tube this contour leads to a 3.5 m funnel to ensure $\alpha = 2°$ along the whole length. Favorably, the centrifuge scatter decreases to $\pm 1°$ for v = 1200 m/s, giving a larger backlog for the impact condition of $\alpha = 2°$

3.3. The Curved Guiding Tube

A curved guiding tube poses two problems to the survival of the pellet - impacts onto the tube wall during collection of the pellet at interfaces such as air-vacuum or funnel-tube discussed above and impacts at turning points inside the tube. The second problem is the relatively long time of interaction between pellet and tube in two areas: mechanical overload through centripetal forces acting on the pellet in bends of the tube and thermal overload through excessive heat exchange.

3.3.1. Impacts at turning points

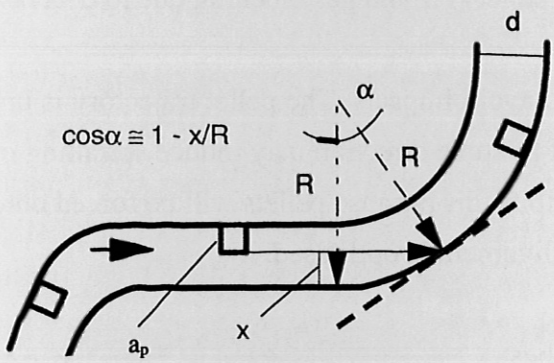

Fig. 16

Schematic of a pellet impact at the turning point of a non-aligned guiding tube.

The schematic in Fig. 16 features the impact of a pellet at a turning point of a curved guiding tube. The pellet is forced to change walls and hits the opposite wall under a considerable angle. Assuming a simple transition from a straight tube into a bent of constant radius, R, the impact angle, α, can be described as a function of R and tube diameter, $d_{in} = x + a_p$:

$$\cos\alpha = 1 - (d_{in} - a_p)/R \qquad (6)$$

Plotting for $a_p = 2$ mm α against d_{in} in Fig.17 emphasizes the strict requirements on tube alignment. Considering the current setup at ASDEX Upgrade ideal alignment was not possible due to limitations in the space available. Therefore the system features no less than 4 turning points with minimum $R \geq 0.35$ m in one bend. Impact angles of over 8° are likely, and the maximum pellet speed of v = 400 m/s reached so far is conceivable.

Clearly, avoiding turning points in the tube trajectory would be ideal and leave only the centripetal load on the pellet. If turning points were inevitable due to space requirements a curved tube optimised for v = 1200 m/s needed $R > 3$ m and $\varnothing_{in} \leq 5$ mm. Even this

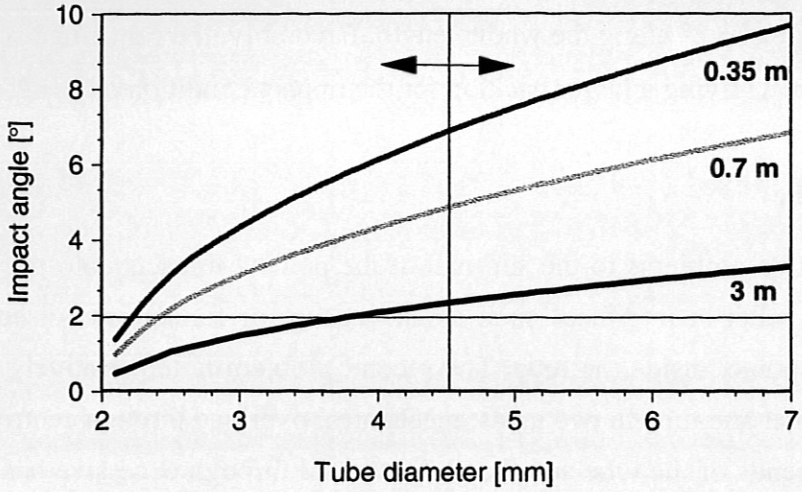

Fig. 17

Plot of impact angle as a function of guiding tube diameter. Radii of curvature are drawn in. The vertical line and the arrow mark the limit of tube diameter > 2x pellet diameter assuming a cubic 2 mm pellet.

requirement could be mitigated by slowly decreasing the radius of the bend from infinity to the needed one. The alternative reduction of the tube diameter should not fall below twice the pellet diameter because of possible mass losses of 40% per pellet /11/ and gas blocking due to decreasing pumping efficiency.

The cross-section of the tube is also crucial to avoid impacts. The pellet trajectory is unpredictable in circular tubes as even slight changes of the tube direction may induce spiralling of the pellet. A tube with a rectangular cross-section inhibits this because pellets will be forced onto another flat surface impact under small angles if the alignment is optimised.

3.3.2. Centrifugal load on pellets in curved guiding tubes

Using the above result that pellets are quasi-sliding with $v_\perp$ = 5 - 10 m/s after impact, the pellet is likely to undergo a few shallow impacts in a curve, loosing perpendicular energy in each of them. Eventually the pellet should slide under full contact (area A) on the tube surface facing a purely centripetal load. The pure load, proportional to curvature, is difficult to measure due the poorly known pellet trajectory after entrance into the tube. Tests of pellets flying into 90°-bends of various radii were performed by Büchl et al /11/ and Combs et al /13/. Both compared the experimental results to a model calculating the minimum possible radius of curvature as a function of pellet mass m, contact area A, centripetal load p, and pellet velocity v:

$$R_{\min} = \frac{m \cdot v^2}{p \cdot A} \qquad (7)$$

It must be noted, that the contact area of a cylindrical pellet is assumed to be the rectangular cross-section of the pellet. Data of both tests are inserted into Fig. 18 where pellet velocity is plotted against radius of curvature and calculated lines of equal contact load for centrifuge pellets are drawn in. Survived pellets at p = 6 bar and p = 10 bar confirm that pellets can handle

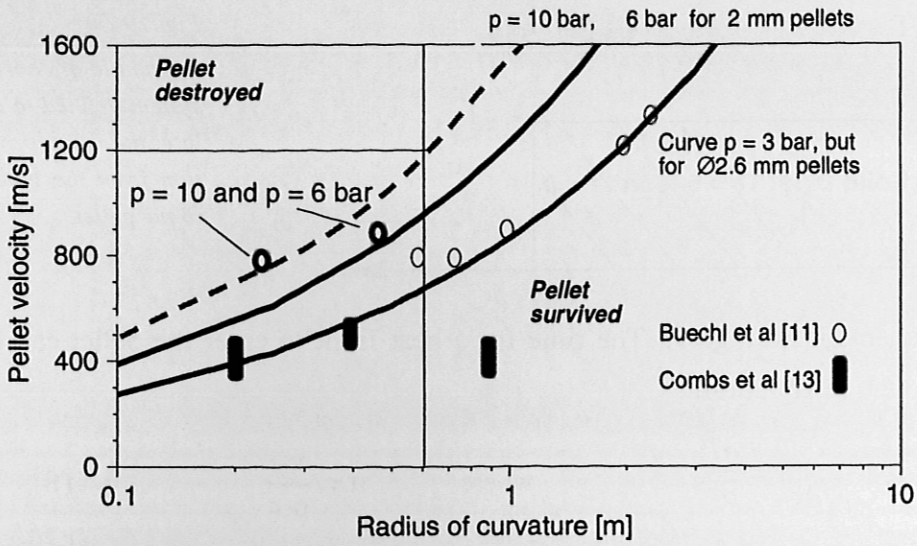

Fig.18 Plot of pellet speed as a function of guiding tube radius. Curves p = 12 and 6 bar are calculated for centrifuge pellets with a_p = 2 mm. The two bold circles at p = 10 and 6 bar belong to Büchl et al /11/.

higher centripetal loads than the statical tension limit measured in /7/. The large spread in experimental data, most points are grouped around p = 3 bar, can be explained by the test set-up. In both studies the pellet was most probably in free flight when entering the test tube and not sliding on the "outward" wall surface prior to the entrance of the 90°-turn. In the majority of shots a not shallow impact ($\alpha > 5°$) occurred distorting the data. In order to measure purely centripetal loads the alignment of the test set up is crucial. The pellet must at least quasi-slide, i.e. fly under a very shallow angle ($\alpha \approx 0.5°$) with respect to the outside of the first bend so as to prevent any "hidden" impact.

In conclusion, the minimum possible radius of curvature for an optimised curved tube can be based on a centripetal load of p = 10 bar on the pellet. The curves drawn into Fig.18 for the centrifuge pellets unveil, that for p = 10 bar v = 1200 m/s becomes accessible at R ≥ 0.6 m. Thus the requirements due to pure centripetal loads in guiding tubes are far less critical than those due to impacts at turning points.

3.3.3. Estimate of thermal pellet-tube wall interaction

The long term (ms-time scale) thermal interaction between pellet and relatively hot tube wall is little understood as yet. For example, in a guiding tube of 20 m length a pellet with v = 500 m/s may be in contact with the tube walls for up to 40 ms. An evaporating gas layer will form due to the Leidenfrost phenomenon /15/ controlling the heat exchange between pellet and tube. This interaction needs a separate study and will be ignored for now. In order to give a rough estimate of the heat penetration into the pellet one can assume the most pessimistic case: direct contact between pellet and tube wall represented here be a heat reservoir at triple point temperature as dis-

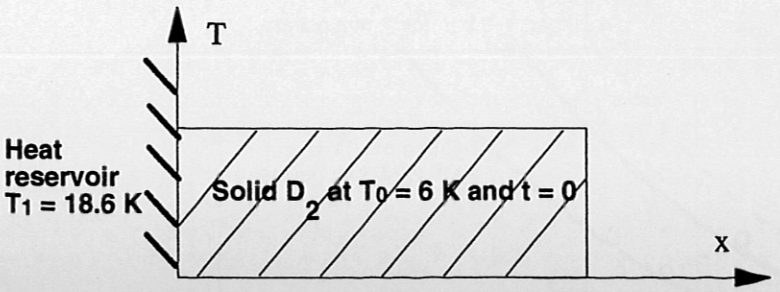

Fig. 19

Schematic of coordinate system defined to calculate the heat propagation from the tube wall to the pellet. .

played in the schematic in Fig.19. The time for a heat front to enter the pellet can be derived from a 1-D conduction equation:

$$\frac{\partial^2 T}{\partial x^2} = \frac{\partial T}{\partial \tau} \qquad \text{where} \qquad \tau = \frac{\kappa \cdot t}{\rho \cdot c} \qquad (8),$$

where κ is the coefficient of thermal conductivity, ρ is the solid density, c the specific heat of D_2. Eq. (8) is solved using the Gaussian error function and obtaining a temperature distribution:

$$T = T_1 + (T_0 - T_1) \cdot \Phi\left(\frac{x}{2} \cdot \tau^{-1/2}\right) \qquad (9),$$

where Φ is the tabulated error integral. Using the cryostat temperature of the centrifuge, T_0 = 6 K, the temperature distribution in the pellet is plotted in Fig.20 for two contact intervals, 10 and 100 ms. Considering the pellet dimension of 2 mm, the penetration curve for 100 ms is consequential because about 20% of the pellet is heated to 12 K, a temperature where the pellet starts to loose tensile strength (Fig.3). Furthermore, in the real tube evaporated gas will not stream off instantaneously but enclose the whole of the pellet. Here perforation of the guiding tube for immediate pump out is required at places where the pellet will definitely make no contact with the tube wall. Only usage of a tube with rectangular cross-section ensures a predictable pellet trajectory.

In conclusion, without taking into account the gas layer between pellet and tube wall a 10 ms transfer time (at v = 1200 m/s tube length l = 12 m) should be aimed for in the optimised guiding system.

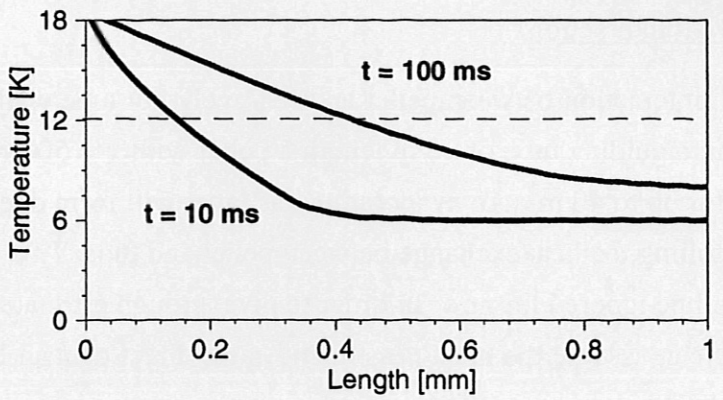

Fig. 20

Plot of the heat propagation into the pellet as a function of time and pellet temperature.

3.4. The Optimised Pellet Guiding System

3.4.1. Geometries of an optimised system

Using the above derived results such as a limiting impact angle of 2°, the quasi-sliding of pellets after grazing incidence impacts, the conditions derived for curved tube alignment (no turning points), tube radii, R > 0.6 m, and rectangular cross-section, the main conclusion of this work can be made. Any pellet guiding system should ensure as few as possible pellet impacts via permanent contact of the pellet with funnel or tube wall achieved by a permanent, however changing, curvature throughout the system. In this sense two basic geometries are proposed for an optimised pellet guiding system to reach v = 1200 m/s on ASDEX Upgrade. They are sketched in Fig.21.

Option 1 is a u-turn in the guiding tube geometry which allows to install the 3.5 m long optimised funnel away from the torus. The centrifuge could stay in place with the firing direction rotated by 180°. The initial width of the rectangular tube needs to be at least 6 mm using the pellet size a_p = 2 mm. The perforated guiding tubes should be kept in a vacuum mantling not shown here. The drawback of this option is a relatively long guiding tube of about 20 m resulting in an overall system length of about 25 m. Option 2 leaves the tube length at 5 m, but its implementation depends on the location of the centrifuge needed to be above ground. In both cases the tube alignment after the funnel is crucial. The pellets are required to quasi-slide or slide as soon as they enter the funnel. Given the technological feasibility the funnel should have a slowly decreasing radius continuing into the tube as shown in Fig.21. Following the concept of a perma-

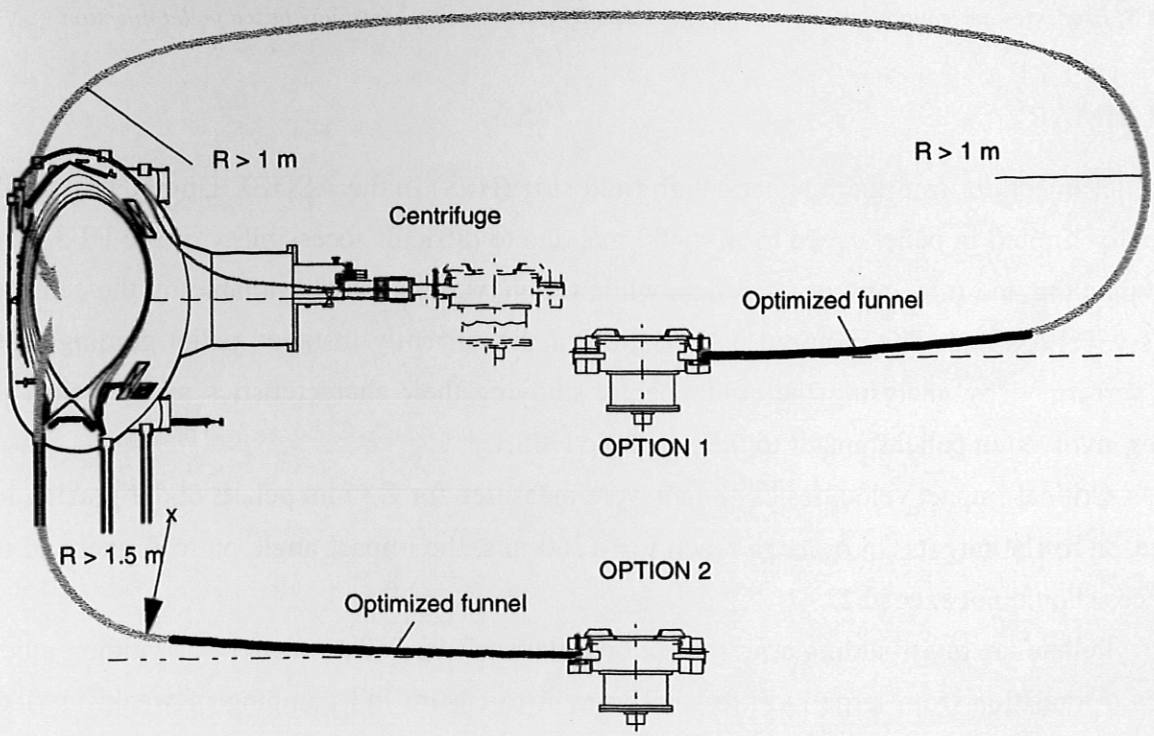

Fig. 21 Schematic of the optimised HFS pellet guiding system at ASDEX Upgrade.

nent tube curvature the middle part of option 1 the tube should remain bent until the entrance to the torus port.

New territory with respect to the efficiency of the high field side injection is the proposed pellet injection angle of ~60° to the horizontal midplane of the torus. The injecting end of the tube should be designed so as to allow some angular variation (e.g. 55° - 65°) via remote control similar to the gas switched control of HFS and LFS injection /4/.

3.4.2. Plasma density control

The length of the guiding tube is important to inhibit a large overshoot of plasma density during pellet injection due to pellets injected after the stop signal has reached the centrifuge. This slow system response is due to several processes two of which are the length of the guiding tube system and the pellet speed. Table 3 highlights the influence of the tube length on the overall system response. As can be seen the currently existing delay can be reduced by a factor 2 - 3 in a system with v = 1200 m/s.

Process	**Current (v = 240 m/s)**	**Option 1 and 2 (v = 1200 m/s)**
Ice transport to cutter	8 ms	8 ms
Ice cutting into pellets	3 ms	3 ms
Pellet flight into stop cylinder	4 ms	4 ms
Synchronisation	0 - 17 ms	0 - 5 ms
Pellet acceleration	20 ms	4 ms
Transfer through funnel + CGT	26 ms at 6.2 m length	17 ms at 20 m, 5.3 ms at 6.3 m
Overall	**61 - 78 ms**	**36 - 41 ms, 24 - 29 ms**

Table 3: Processes determining the sensitivity of the density control using centrifuge based pellet injection

4. SUMMARY

D_2-pellet injection from the magnetic high field side (HFS) in the ASDEX Upgrade tokamak is currently limited in pellet speed to $v < 400$ m/s due to difficult accessibility of the HFS requiring funneling and tube guiding of pellets while the maximum speed available by the centrifuge /4/ is v = 1200 m/s. The required optimisation of the currently installed pellet guiding system was performed by analysing the components, studying their characteristics and physical processes involved in pellet transfer to the magnetic HFS.

Critical impact velocities of 48 m/s were measured for ∅3 mm pellets under grazing incidence on to flat targets. In order to reach v = 1200 m/s, the impact angle on to funnel and tube surfaces should not exceed 2°.

Pellets are quasi-sliding after impact on a flat surface. Pellet transfer in a guiding tube requires a transition from large radii to smaller radii to ensure full damping of weakly reflected pellets. It is possible to devise a guiding system with at most two impacts of $\alpha \leq 2°$, one in the

funnel and one at the air-vacuum interface.

The cross-section of the curved guiding tubes needs to be rectangular. Radii should be R > 1 m to reach v = 1200 m/s if there are no turning points, and 3 m if turning points can not be avoided. The tube length should be not more than 20 m and perforated to avoid large mass losses due to melting pellets and possible gas blocking.

A future pellet guiding system was devised based on a permanent curvature of both, funnel and guiding to tube to force the pellets into a permanent sliding. The system includes a 3.5 m long funnel to capture the pellets, and a u-turn in the guiding tube geometry which allows to install the funnel away from the congested torus area. Despite a relatively long guiding tube of about 20 m the pellets travel through the whole guiding system at v = 1200 m/s in about 35 ms which enables more than twice as fast density control as in the current configuration.

5. OUTLOOK

Impact tests will be performed applying controlled implantations of 0.1%, 0.2%, 0.5% N_2 into D_2 expected to lead to an increase in pellet strength of 1.2 - 1.5 times /8/. On the other hand, tests with pure D_2 should establish, whether impurities in the impact tests reported above (0.2% HD, traces of N_2 and O_2) are responsible for the difference in v_c to tests made by Combs et al. /13/. The influence of the ortho-para-ratio /14/ on the strength of cryogenic D_2 also needs to be studied experimentally.

The interaction between pellet and target could not be established unambiguously in this work. Schlieren photography in the same orientation before, during and after the impact will enable measurements of the pellet size and shape before and after the impact as well as the amount of material shaved off the pellet during the impact. The appearance of cracks may be recorded to understand the propagation of a stress wave in the pellet as a possible source of destruction.

The phenomenon of the insulating vapor layer between pellet and tube wall surface should be studied experimentally and numerically. Measurements of the mass loss in a guiding tube are in preparation using microwave resonators shortly after beginning and before the end of a bend. In the tests the mass loss of perforated tubes should be compared with that closed tubes. Exact knowledge of the mass loss will also enable computation of the thickness of the gas layer. Simultaneously, the formation and dynamics of the gas layer as a self-regulating process should be estimated in a numerical simulation.

REFERENCES

/1/ V. Mertens et al., Proc. 24th IAEA-conference, Yokohama (1998) to be published

/2/ P.T. Lang et al, Report IPP1/314, Max-Planck-Institut f. Plasmaphysik (1998)

/3/ M. Kaufmann et al, Nucl. Fusion, **26**(2), 171 (1986)

/4/ C. Andelfinger et al, Rev. Scient. Instr., **64**(4), 983 (1993)

/5/ P.T. Lang et al., Phys. Rev. Lett. **79**, 1487 (1997)

/6/ P.T. Lang et al., Proc. of 20th Symposium On Fusion Technology, Marseille, Vol.2, p.1025, Association Euratom - CEA (1998)

/7/ Bolschyutkin et al., Soviet Physics - Solid State, **12**(1), 119 (1970)

/8/ L.A. Alexeeva and M.N. Kazeev, Workshop on Refueling of Fusion Plasmas, Kurchatov Inst. of Atomic Energy Moscow (1990)

/9/ Fa. Linde, private communication.

/10/ W. Riedmüller, IPP 4/188, Max-Planck-Institut f. Plasmaphysik (1980)

/11/ K. Büchl and W. Sandmann, Fusion Technology 1982, Proc. 12th Symposium Jülich, Vol.2, Oxford, Pergamon Press, 1982, p.1507 & C. Andelfinger et al., Report IPP1/219, Max-Planck-Institut f. Plasmaphysik (1983)

/12/ M. Thöner, Report IPP1/207, Max-Planck-Institut f. Plasmaphysik (1982)

/13/ S. Combs et al, Proc. of Ann. Meeting of ANS, Nashville, to appear in Fusion Technology (1998)

/14/ P.C. Souers, Hydrogen Properties for Fusion Energy, Univ. of California Press (1986)

/15/ B.S. Gottfried et al., Int. J. Heat Mass Transfer, **9**, 1167 (1966)